Epitaxial strain effect on transport properties in $Ca_{2-x}Sr_xRuO_4$ thin films

Ludi Miao, Wenyong Zhang, Punam Silwal, Xiaolan Zhou, Ilan Stern, Tijiang Liu, Jin Peng, Jin Hu, Dae Ho Kim, and Z. Q. Mao*

Department of Physics and Engineering Physics, Tulane University, New Orleans, Louisiana 70118, USA

(Received 15 May 2013; revised manuscript received 19 July 2013; published 3 September 2013)

We have grown $Ca_{2-x}Sr_xRuO_4$ ($x = 0$, 0.1, 0.5, and 2) epitaxial thin films using a pulsed laser deposition method and characterized their structures and magnetotransport properties. We find that the $x = 0$, 0.1, and 0.5 films grown on $LaAlO_3$ substrates exhibit coherent strain with tetragonal structure. The nature of strain is dependent on Sr content: the Ca_2RuO_4 ($x = 0$) film features biaxial compressive strain, while the $x = 0.5$ film shows biaxial tensile strain. The strain in the $x = 0.1$ film is relatively weak and strongly anisotropic, with compressive strain along the a axis and tensile strain along the b axis. In contrast, the Sr_2RuO_4 films show strain relaxation. The epitaxial strain effect leads the properties of the $x = 0$, 0.1, and 0.5 films to be distinct from those of bulk materials. The bulk material shows antiferromagnetic Mott-insulating properties for $x < 0.2$ and a nearly ferromagnetic state for $x \sim 0.5$ [Nakatsuji and Maeno, Phys. Rev. Lett. **84**, 2666 (2000)], whereas the film displays itinerant ferromagnetism for $x = 0$ and 0.1 and paramagnetic metal for $x = 0.5$. Furthermore, in the $x = 0$ and 0.1 films, we observed distinct fourfold ferromagnetic anisotropy, with the minimum magnetoresistivity along the diagonal directions for $x = 0$ and a and b directions for $x = 0.1$. Such evolution of magnetic anisotropy may be associated with the tuning of the spin-orbit coupling by the epitaxial strain.

DOI: 10.1103/PhysRevB.88.115102 PACS number(s): 73.50.−h, 81.15.Aa, 71.27.+a

I. INTRODUCTION

Strongly correlated Ruddlesden-Popper (RP) series of ruthenates, $(Ca,Sr)_{n+1}Ru_nO_{3n+1}$ exhibit a rich variety of fascinating properties, such as spin-triplet superconductivity in Sr_2RuO_4 (SRO),[1–3] antiferromagnetic (AFM) Mott-insulating state in Ca_2RuO_4 (CRO),[4–6] itinerant ferromagnetism in $SrRuO_3$,[7] a field-tuned electronic nematic phase in $Sr_3Ru_2O_7$,[8] and colossal magnetoresistance induced by the spin-valve effect in $Ca_3Ru_2O_7$.[9,10] The close proximity of these exotic properties reflects competing physical interactions of comparable strength between spin, charge, lattice, and orbital degrees of freedom in ruthenates. Such competing interactions lead the properties of ruthenates to be susceptible to external stimuli; nonthermal parameters such as hydrostatic pressure,[11,12] magnetic field,[8–10] and chemical substitution[13–15] can readily tune the ruthenates to various ground states.

One remarkable example is the single-layered $Ca_{2-x}Sr_xRuO_4$ (CSRO) solid solution series,[13,14] where Sr substitution for Ca results in diverse electronic and magnetic states. With the increase of Sr content, the system evolves from the AFM Mott-insulating state for $0 \leqslant x < 0.2$ to a metallic state with short-range AFM correlations, to a nearly ferromagnetic (FM) state for $x \sim 0.5$, then to a paramagnetic metallic state for $0.5 < x < 2$, and finally to a spin-triplet superconductor for $x = 2$. Such drastic changes in the physical properties of CSRO have been attributed to the lattice distortion caused by the substitution. Since Ca^{2+} has a smaller ionic radius than Sr^{2+}, Ca^{2+} substitution for Sr^{2+} leads to RuO_6 octahedral rotation for $0.5 \leqslant x < 1.5$ and simultaneous rotation and tilting for $0 \leqslant x < 0.5$.[16] First-principles calculations revealed that the RuO_6 octahedral rotation is responsible for the enhanced FM fluctuations near $x \sim 0.5$, whereas the RuO_6 octahedral tilting favors AFM correlation for $x < 0.5$.[17]

Aside from chemical substitution, CRO was also found to be susceptible to hydrostatic/uniaxial pressure[11,12,18] and epitaxial strain.[19,20] When the hydrostatic pressure applied on a bulk CRO single crystal is above 0.5 GPa, its ground state evolves from the AFM Mott-insulating state to an itinerant FM state.[12] A metal-insulator (MI) transition can also be triggered by in-plane uniaxial pressure, with the critical pressure being about 1.5 GPa. Structure studies by neutron scattering experiments showed that the ferromagnetism under pressure originates from the decrease of the RuO_6 octahedral tilting angle,[21] consistent with the dependence of magnetic correlation on the structural distortion seen in the CSRO bulk materials. In the CRO epitaxial films grown on $LaAlO_3$ (LAO) (001) substrates,[19,20] the lattice mismatch between CRO and LAO produces compressive strain along the in-plane directions, resulting in a tetragonal structure in the CRO film. The change from the orthorhombic structure in CRO bulk to the tetragonal structure in the CRO film suggests that the epitaxial strain also suppresses the RuO_6 octahedral tilting, similar to the effect generated by the hydrostatic pressure. Such an epitaxial strain effect not only suppresses the MI transition but also causes itinerant ferromagnetism with $T_C = 18$ K.[20]

Given that CSRO and its end members have such rich interesting physics and their properties are sensitive to external stimuli, we have investigated the properties of these materials using epitaxial thin-film samples grown by the pulsed laser deposition (PLD) method. Our motivation is to examine the effect of epitaxial strain on the properties of CSRO. In this article, we report the growth of CRO, CSRO, and SRO films on various substrates, as well as their structural characteristics and magnetotransport properties. We find that the CRO and CSRO ($x = 0.1$ and 0.5) films on LAO substrates feature coherent epitaxial strain, whereas the SRO ($x = 2$) films show almost complete strain relaxation. Like the epitaxial strain effect observed in the parent compound CRO,[20] the epitaxial strain on the CSRO films also leads their properties to be distinct from those of bulk materials. In the $x = 0.1$ sample, we observe itinerant ferromagnetism similar to that seen in the CRO

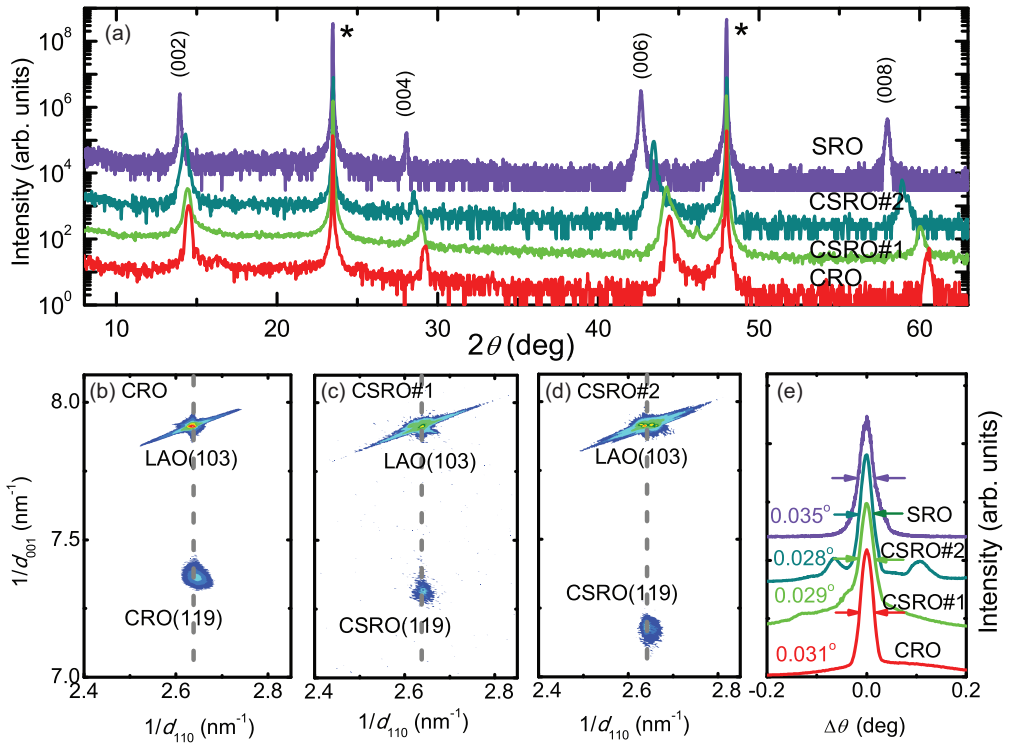

FIG. 1. (Color online) (a) HR-XRD 2θ-θ scan of 50-nm CSRO films with $x = 0$, 0.1, 0.5, and 2 on (001) LAO substrates. The stars indicate LAO reflection peaks. RSMs of HR-XRD around the LAO (103) peaks and the (119) peaks of (b) CRO with $x = 0$, (c) CSRO#1 with $x = 0.1$, and (d) CSRO#2 with $x = 0.5$. (e) Rocking curves around the (002) reflections of the films with $x = 0$, 0.1, 0.5, and 2 (the data has been shifted for clarity).

film. This FM state is characterized by a fourfold magnetic anisotropy with the minimum magnetoresistivity along [100] and [010] directions. This is in contrast with the fourfold magnetic anisotropy with the minimum magnetoresistivity along the [110] and [1-10] directions in FM state of the CRO film. The $x = 0.5$ film shows paramagnetic behavior with a Fermi-liquid ground state as compared to the nearly FM non-Fermi liquidlike state for $x = 0.5$ bulk crystal. We will show these exotic properties on CSRO films can be understood in terms of the control of RuO_6 octahedral rotation and tilting by the epitaxial strain.

II. EXPERIMENT

The CRO, CSRO, and SRO thin films were grown using the PLD method with a KrF excimer laser ($\lambda = 248$ nm).[20] The energy density of the laser pulse used for growth is 1.0 J/cm^2. For CRO and CSRO growth, we tried using various substrates, but successful growth was made only on LAO substrates. However, SRO can be grown on various substrates, including LAO, LSGO ($LaSrGaO_4$), NGO ($NdGaO_3$), LSAT [$(LaAlO_3)_{0.3}(SrAl_{0.5}Ta_{0.5}O_3)_{0.7}$], and STO ($SrTiO_3$). This is consistent with previous reports on SRO growth.[22–27] All substrates used in our growth have (001) pseudocubic orientations. $Sr_3Ru_2O_7$ and $Ca_3Ru_2O_7$ single crystals (grown by the floating zone method[28]) were used as targets for SRO and CRO growth. The use of target materials with double-layered phases instead of the intended single layered phases was to allow excess Ru in the target to compensate its loss during the ablation.[20] The CRO films were deposited at 1120 °C in the atmosphere of 5 mTorr of O_2 and the SRO films at 1120 °C in 1 mTorr of mixed gas (1% O_2 and 99% Ar). Such high deposition temperature allows fast growth rate, ~0.57 nm/sec for a laser repetition rate of 10 Hz. The CSRO films with $x = 0.1$ and $x = 0.5$ were grown using polycrystalline targets with 20% of excess Ru, since it is difficult to make large single crystals of double-layered phase for these compositions. They were deposited at 990 °C in 1 mTorr of O_2 at a slow growth rate, with ~0.11 nm/sec with a laser repetition rate of 2 Hz. The CRO and CSRO films are 50 nm thick, whereas the thickness of the SRO films is in the 50–150 nm range. The structural and magnetic properties of films were characterized by a high-resolution four-circle x-ray diffraction (HR-XRD, Bruker) and a superconducting quantum interference device (Quantum Design), respectively. The electronic transport properties of films were measured using a standard four-probe method in a Physical Property Measurement System (PPMS, Quantum Design).

III. RESULTS AND DISCUSSIONS

In Fig. 1, we present the XRD data of the films on LAO substrates for $x = 0$ (CRO), 0.1 (CSRO#1), 0.5 (CSRO#2), and 2 (SRO). These films show high quality of crystallization with c orientation, which can be seen clearly from the strong (00l) diffraction peaks in the 2θ-θ scans shown in Fig. 1(a). For CSRO#1, we also observed an additional, weak peak around $2\theta = 46°$, which is possibly due to

TABLE I. Lattice constants and strain of CSRO films with $x = 0, 0.1, 0.5$, and 2. All these films have a thickness of 50 nm and are grown on pseudocubic LAO_3 substrates with (001) orientation and lattice constant $a_{LAO} = 5.3599/\sqrt{2}$ Å. a_{bulk}, b_{bulk}, and c_{bulk} denote the lattice constants of bulk materials, whereas a_{film} and c_{film} denote the lattice constants of thin films. ε_a, ε_b, ε_{ave}, and τ denote the strain of the films along a and b axes, the average strength of the strain, and the anisotropy of the strain, respectively. The doubling of the c lattice constant for the $x = 0.5$ bulk material is due to the rotation pattern of RuO_6 octahedra.[16]

x	a_{bulk} (Å)	b_{bulk} (Å)	c_{bulk} (Å)	a_{film} (Å)	c_{film} (Å)	ε_a (%)	ε_b (%)	ε_{ave} (%)	τ (%)
0	5.4097(3)[29]	5.4924(4)[29]	11.9613(6)[29]	5.341(5)	12.23(0)	−1.26	−2.75	−2.01	1.49
0.1	5.3494(3)[16]	5.3420(3)[16]	12.3219(4)[16]	5.344(3)	12.30(1)	−0.10	+0.04	−0.03	0.14
0.5	5.3395(1)[16]	"	2×12.5749(3)[16]	5.359(9)	12.54(2)	+0.38	"	+0.38	0
2	5.47443(3)/$\sqrt{2}$[30]	"	12.7397(4)[30]	5.498(5)	12.71(3)	+0.47	"	+0.47	0

intergrowth of minor (Sr,Ca)RuO_3 phase. The full widths at half maximum (FWHMs) $\Delta\theta_{FWHM}$ of the rocking curves of the (002) reflection peaks are as sharp as ∼0.028–0.035° for all these films, as shown in Fig. 1(e). The satellite peaks near the (002) reflection in the rocking curve of CSRO#2 should be attributed to other domains in the films, which arise from twin domains in commercial LAO substrates. From the XRD ϕ scans for CRO (SRO or CSRO) (113) and LAO (101) reflections (data not shown here), fourfold symmetries are observed, indicating the epitaxial growth with $[001]_{film}\|[001]_{LAO}$ and $[110]_{film}\|[100]_{LAO}$. The diffraction indices denoted in Fig. 1 are based on the pseudotetragonal unit cell with $a \approx b \approx \sqrt{2} \times a_0$ (a_0, the distance between a Ru^{4+} ion and its nearest neighboring Ru^{4+} ion).

We have also performed XRD reciprocal space map (RSM) measurements on the CRO, CSRO#1, and CSRO#2 films on LAO substrates, as shown in Figs. 1(b)–1(d). The single (119) diffraction spot of the CRO or CSRO film indicates that all these films are free of twinning domains and possess tetragonal lattices.[20] From the horizontal and vertical peak positions in RSM, the lattice parameters a and c can be calculated, as summarized in Table I where the lattice parameters of bulk materials with the same compositions are also given for comparison. The lattice parameter a of the film hardly changes with Sr substitution for Ca for both CSRO#1 and CSRO#2, and it stays close to that of LAO substrate, which can be seen clearly from the vertical alignment between the LAO (103) and the CRO (or CSRO) (119) diffraction spots in Figs. 1(b)–1(d). This indicates that the CRO or CSRO films are grown with almost coherent strain. We also note that the c lattice parameter of CSRO films increases with Sr content (see Table I), consistent with the trend observed in bulk CSRO.[16]

From the lattice parameters of bulk materials[16,29] and thin films, we have evaluated the epitaxial strain of the CRO and CSRO films along in-plane crystallographic directions, which is defined as $\varepsilon_a(x) = \frac{a_{film}(x) - a_{bulk}(x)}{a_{bulk}(x)}$ and $\varepsilon_b(x) = \frac{b_{film}(x) - b_{bulk}(x)}{b_{bulk}(x)}$, with the average strength of strain $\varepsilon_{ave}(x) = \frac{\varepsilon_a(x) + \varepsilon_b(x)}{2}$. As shown in Table I, ε_a, ε_b, and ε_{ave} are negative with relatively large magnitudes (i.e., −1.26%, −2.75%, and −2.01%, respectively) for CRO, indicating biaxial compressive strain. In CSRO#1, ε_a, ε_b, and ε_{ave} decrease to small magnitudes with mixed signs (i.e., −0.1%, +0.04%, −0.03% respectively), indicating weak compressive strain along the a axis and slight tensile strain along the b axis. In contrast, ε_a, ε_b, and ε_{ave} all become positive for CSRO#2, with an identical magnitude (i.e., 0.38%), indicating biaxial tensile strain. Such evolution of epitaxial strain with Sr content agrees well with the fact that the lattice parameter a of the LAO substrate is smaller than that of bulk CRO but greater than that of the bulk CSRO with $x = 0.5$. From Table I, we can see that the lattice parameter c of the CRO film is remarkably greater than that of bulk CRO, whereas in $x = 0.5$ film, the c lattice parameter is less than that of the $x = 0.5$ bulk material. This result is consistent with the general expectation that the compressive strain should elongate the c axis, while the tensile strain should shorten the c axis. Furthermore, we have also examined the anisotropy of epitaxial strain, defined as $\tau = |\varepsilon_a - \varepsilon_b|$, for these films. As shown in Table I, τ is ∼1.49% for $x = 0$; it decreases with Sr substitution, down to zero for $x = 0.5$. Such a decrease of strain anisotropy can be well understood in light of the bulk structural evolution from orthorhombic for $x < 0.5$ to tetragonal for $x \sim 0.5$.[16] Since τ is associated with the structural confinement that the pseudocubic LAO substrate

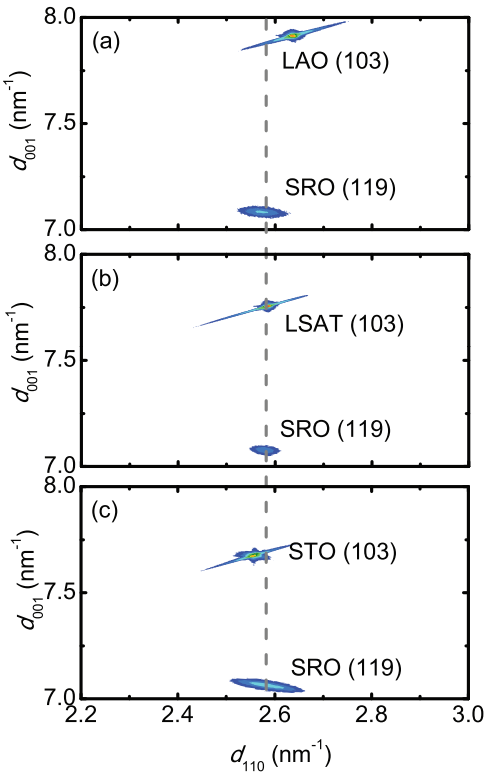

FIG. 2. (Color online) HR-XRD RSMs around (119) reflections of SRO films on (a) LAO, (b) LSAT, and (c) STO substrates.

imposes on the film, τ is naturally expected to be zero when the bulk material possesses tetragonal structure for $x \geqslant 0.5$.

In contrast with the strained CRO or CSRO films, all of the SRO films on various substrates show strain relaxation, which is clearly manifested in the RSMs. Figure 2 presents the data for SRO/LAO, SRO/LSAT, and SRO/STO films. The SRO (119) diffraction spots of these films share an almost identical position along the horizontal directions in RSM, indicating strain relaxation. The in-plane lattice parameter a of these films are found to be nearly identical to that of bulk SRO, in spite of the 0.05–2.1% difference in a between bulk SRO and these three substrates. Since the LSAT substrate has the least difference (0.05%) in the lattice parameter a from bulk SRO, the SRO (119) diffraction spot looks nearly aligned with the LSAT (103) spot. The SRO thin films on LSGO and NGO substrates exhibit similar strain relaxation as the SRO/LAO, SRO/STO, and SRO/LSAT films do. The strain-resistant nature of SRO films can be understood as follows: In SRO, the RuO_6 octahedra do not involve any rotation and tilting, thus yielding a relatively stiff structure; however, in CRO the tilted, rotated RuO_6 octahedra allow more active lattice degree of freedom,[30] yielding relatively soft structure.

Although the SRO films on various substrates have nearly the identical lattice parameter a, we find that the rocking curve of the SRO (002) reflection is strongly dependent on the lattice mismatch between the SRO films and the substrates, as shown in Fig. 3. Large $\Delta\theta_{\mathrm{FWHM}}$ is observed in the films with greater lattice mismatch, such as the SRO/LAO and SRO/STO films, whereas the smallest $\Delta\theta_{\mathrm{FWHM}}$ is observed in the film with the least lattice mismatch, i.e., the SRO/LSAT film. Since $\Delta\theta_{\mathrm{FWHM}}$ characterizes the crystalline mosaic spread of the films, the substrate dependence of $\Delta\theta_{\mathrm{FWHM}}$ in Fig. 3 could be understood in terms of the crystalline dislocations generated by lattice mismatch, which is ubiquitous in strain-relaxed thin films.[31,32] We note that Krockenberger *et al.*[26] recently reported superconductivity on SRO/LSAT thin film. This is in line with our observation that the SRO/LSAT film has the least degree of disorders compared to SRO thin films on other substrates.

We have characterized electronic transport properties of the CRO, CSRO, and SRO thin films discussed above. Figure 4(a) presents the in-plane resistivity ρ_{ab} as a function of temperature T for the CRO and CSRO films. Unlike the

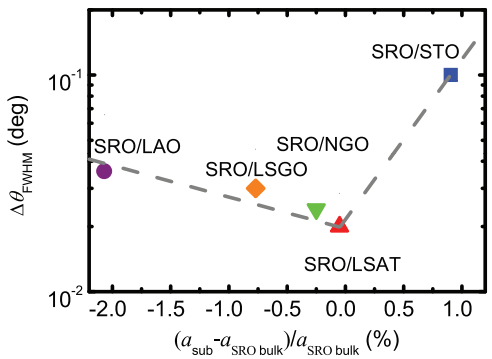

FIG. 3. (Color online) FWHMs of the SRO (002) rocking curve, $\Delta\theta_{\mathrm{FWHM}}$, as a function of the lattice mismatch for SRO films on various substrates.

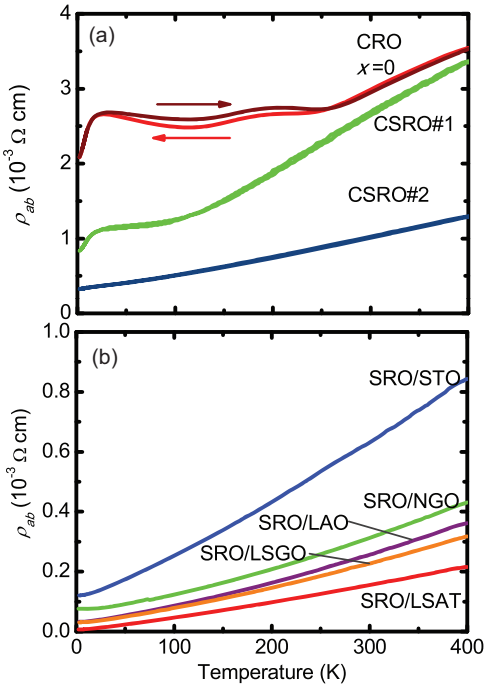

FIG. 4. (Color online) (a) In-plane resistivity ρ_{ab} vs temperature for CRO, CSRO#1 ($x = 0.1$), and CSRO#2 ($x = 0.5$) films. The arrows indicate warming and cooling. (b) In-plane resistivity ρ_{ab} vs temperature for SRO films grown on LAO, LSGO, NGO, LSAT, and STO substrates.

strong first-order MI transition at 350 K in bulk CRO,[4,5] the MI transition is strongly suppressed in the strained CRO/LAO film with T_{MI} shifting down to 250 K, and ρ_{ab} exhibits less insulating behavior below T_{MI} than our previously reported 170-nm CRO film, where $T_{\mathrm{MI}} \sim 300$ K.[20] This suggests that the strain effect weakens with an increase of film thickness, which is common in epitaxial thin films. The current CRO

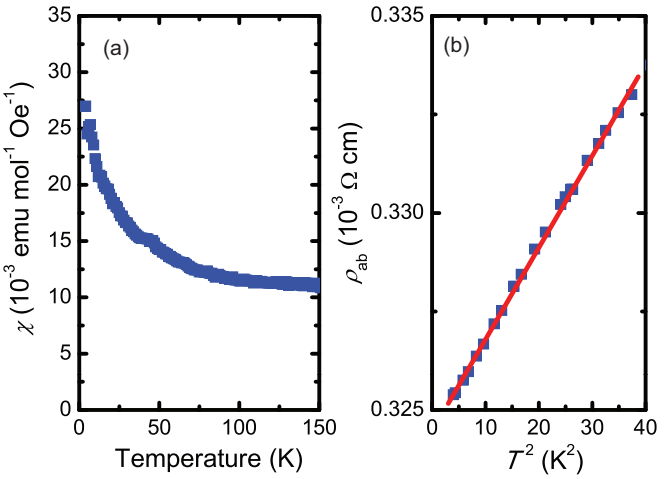

FIG. 5. (Color online) (a) Susceptibility vs temperature for CSRO#2, measured with a magnetic field of 1 kOe, along $[110]_{\mathrm{CSRO}}$. These data are acquired by subtracting the susceptibility of the bare LAO substrate obtained by polishing off the CSRO film from the overall susceptibility data of the film and substrate. (b) In-plane resistivity ρ_{ab} vs T^2 for CSRO#2.

film also shows a resistivity drop near 18 K as in the previous 170-nm-thick film, which is associated with an itinerant FM transition.[20] Such suppression of MI transition caused by epitaxial strain can be attributed to the structural confinement effect imposed by the LAO substrate, which hinders the presence of the tetragonal-orthorhombic structural transition.[20] The MI transition suppression by the epitaxial strain effect also occurs in the CSRO#1 film. For this sample, ρ_{ab} exhibits metallic behavior in the completely measured temperature region, although the $x = 0.1$ CSRO bulk material shows a first-order MI transition at 110 K.[13] This sample shows a slight resistivity drop below 18 K as well, suggesting the presence of itinerant ferromagnetism as in the CRO thin film sample; this is verified from magnetoresistivity measurements as shown below. Compared to CSRO#1, the sample CSRO#2 is more metallic and does not show any resistivity drop related to ferromagnetism at low temperature. We have pointed out previously that the bulk CSRO with $x \sim 0.5$ reaches a nearly FM state.[13,14] Given that the epitaxial strain drives a FM order in both CRO and CSRO#1 films, we would expect that the FM correlation in CSRO#2 should be further enhanced by the strain. However, as shown in Fig. 5(a), the temperature dependence of susceptibility χ of CSRO#2 exhibits paramagnetic behavior. The susceptibility value in $T \rightarrow 0$ K limit, $\chi(0)$, is ~27 memu/(mol-Ru Oe), much smaller than that of the $x = 0.5$ bulk crystal where $\chi(0) =$ 125 memu/(mol-Ru Oe),[13] indicating suppressed magnetic fluctuations for the $x = 0.5$ film. In Fig. 5(b), we show the plot of in-plane resistivity ρ_{ab} vs T^2 for CSRO#2. The T-squared dependence of ρ_{ab} below 6 K, as indicated by the fitting curve reflects Fermi liquid behavior, in contrast with the non-Fermi liquid behavior seen in the resistivity of $x = 0.5$ bulk single crystals, where $\rho_{ab} \propto T^{1.4}$.[13] Given that the non-Fermi-liquid behavior in the $x = 0.5$ bulk crystal is associated with enhanced spin fluctuations,[13] our observation of Fermi liquid behavior in the resistivity of CSRO#2 suggests that magnetic fluctuations are weakened by the tensile strain, consistent with the result of susceptibility measurements mentioned above.

The resistivity data of the SRO films on various substrates are presented in Fig. 4(b). All of them exhibit comparable, metallic temperature dependences, consistent with early reports on SRO films.[22–26] We note that the SRO/STO film has the largest residual resistivity (118 $\mu\Omega$ cm), while the SRO/LSAT film has the least residual resistivity (6 $\mu\Omega$ cm). This is consistent with the structural characteristics of these films. As shown in Fig. 3, the SRO/STO has the largest value of $\Delta\theta_{\mathrm{FWHM}}$, whereas the SRO/LSAT has the smallest $\Delta\theta_{\mathrm{FWHM}}$; this indicates that the degree of disorders is the highest in the SRO/STO film and the least in the SRO/LSAT film. Strong disorders would certainly cause a high scattering rate, resulting in high residual resistivity. Since the SRO is strain resistant as discussed above, the degree of disorders depends on the lattice mismatch. For the SRO/LSAT film, we measured its resistivity down to the millidegrees Kelvin range in a dilution refrigerator but did not observe superconductivity. The disorder scattering should account for the superconducting pair breaking in the SRO films.

To further investigate the relationship between the electronic transport and magnetism in CRO and CSRO films, we have performed angle-resolved in-plane magnetoresistivity (AMR) measurements on these films. AMR has been proven effective in providing valuable information on the anisotropic properties of a magnetic state.[20,33] Figures 6(a)–6(c) present the polar plots of AMR (ϕ,T), defined as $\frac{\rho_{ab}(\phi,T,H)-\rho_{ab}(\phi,T,0)}{\rho_{ab}(\phi,T,0)}$, at various temperatures for the CRO, CSRO#1, and CSRO#2 films, where ϕ is the azimuthal angle. Similar to the results we reported for the 170 nm CRO/LAO film in Ref. 20, the AMR (ϕ,T) of the current 50-nm CRO film also exhibits a crossover from twofold magnetic anisotropy to fourfold anisotropy when the temperature is lowered below 18 K, where ρ_{ab} shows a drop. From the discussions given in Ref. 20, the twofold anisotropy above T_C should be attributed to the insulating AFM order, whereas the fourfold anisotropy below T_C could be viewed as a signature for the FM phase. We also observed a similar crossover from twofold to fourfold anisotropy in AMR (ϕ,T) near 18 K in CSRO#1, suggesting that the epitaxial strain in this sample, while it is weaker than the CRO film, induces ferromagnetism as well. However, we notice that the minimum magnetoresistivity of this sample occurs along the [100] or [010] direction, in contrast with the CRO film which shows minimum magnetoresistivity along the [110] or [1–10] direction. This will be discussed in more detail below. For CSRO#2, AMR (ϕ,T) did not show fourfold anisotropy at low temperatures and only very weak twofold anisotropy was

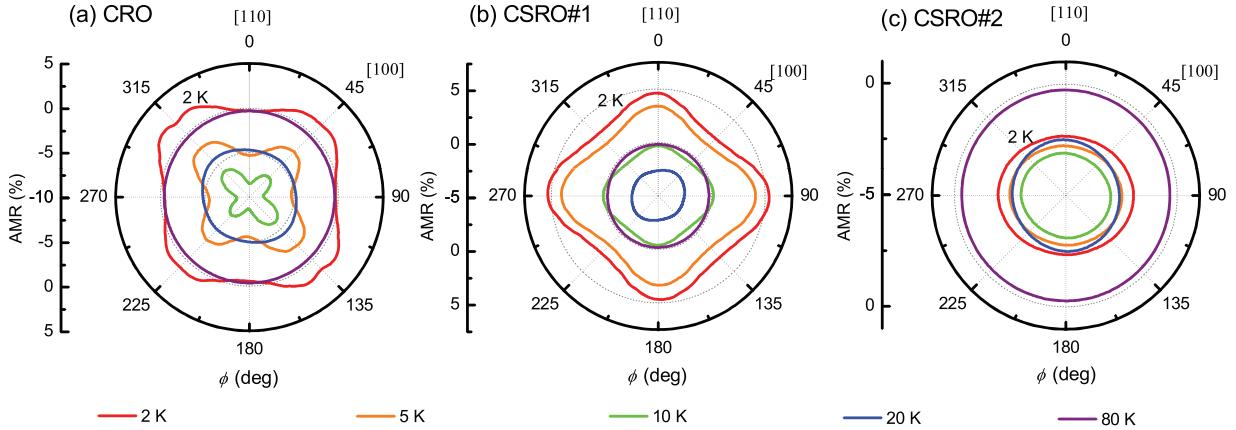

FIG. 6. (Color online) In-plane angular dependence of normalized intraplanar magnetoresistance AMR $= [\rho_{ab}(T,H) - \rho_{ab}(T,0)]/\rho_{ab}(T,0)$ of (a) CRO, (b) CSRO#1 with $x = 0.1$, and (c) CSRO#2 with $x = 0.5$ thin films at various temperatures and at a fixed field of $\mu_0 H = 8$ T.

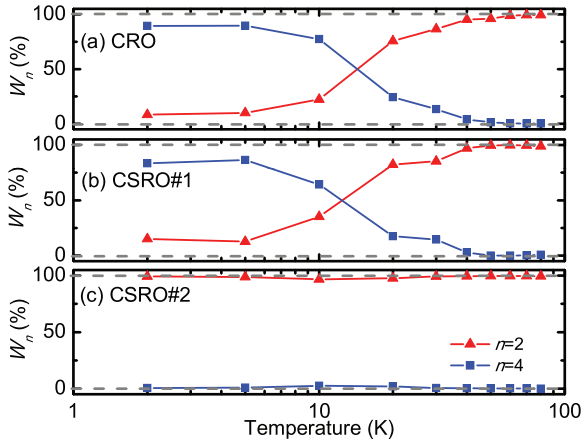

FIG. 7. (Color online) Twofold squared weight W_2 and fourfold squared weight W_4 defined as $W_n(T) = |A_n(T)|^2 / \sum_n |A_n(T)|^2$, as a function of temperature for (a) CRO, (b) CSRO#1 with $x = 0.1$, and (c) CSRO#2 with $x = 0.5$.

observed, consistent with the paramagnetic behavior probed in susceptibility [see Fig. 5(a)]. In order to evaluate the extrinsic anisotropy of AMR arising from the misalignment of the magnetic field out of the conducting plane, we measured AMR as a function of polar angle θ for CRO, which shows a twofold anisotropy with an amplitude AMR_θ of ~7% (data not shown here). Since the field misalignment angle for a thin-film sample mounted on the PPMS rotating sample stage is estimated to be ~0.2°, the amplitude of the extrinsic twofold AMR anisotropy from the field misalignment effect for our thin-film samples is $\sim\text{AMR}_\theta \times (\sin 0.2\ ^\circ) = 0.02\%$, much less than the observed azimuthal AMR amplitudes for CRO (2%), CSRO#1 (2%), and CSRO#2 (0.36%).

We have performed Fourier transform analyses for the AMR (ϕ) data in Fig. 6. In Figs. 7(a)–7(c), we present the squared weights of twofold and fourfold symmetries as a function of temperature T, respectively for CRO, CSRO#1, and CSRO#2 films. The n-fold normalized square weight is defined as $W_n(T) = |A_n(T)|^2 / \sum_n |A_n(T)|^2$, where $A_n(T) = \frac{1}{2\pi}\int_0^{2\pi} \text{AMR}(\phi, T)\exp(-in\phi)d\phi$ is the n-fold complex amplitude. The variations of W_2 and W_4 with temperature look similar between CRO and CSRO#1: the W_2 stay at ~15% in the ground state and increase to nearly 100% above T_C = 18 K, while W_4 stay at around 85% below T_C and decrease to nearly 0% as the temperature is increased above T_C. This indicates that the $x = 0$ and 0.1 films have a similar magnetic ground state with coexistence of AFM and FM below T_C. For CSRO#2, in contrast, W_2 stays at ~100% with negligible W_4 throughout the measured temperature range (2–80 K). The twofold anisotropy of this sample has a very small amplitude compared to the twofold anisotropies seen in the CRO and CSRO#1 samples and could be attributed to an enhanced paramagnetic state.

Although the CSRO#1 sample shares a similar magnetic ground state with the CRO sample as suggested above, their fourfold anisotropy in AMR (ϕ) shows a $\pi/4$ phase shift (see Fig. 6). This can probably be understood as follows. In general, what AMR anisotropy reflects is actually magnetocrystalline anisotropy; this has been established in theory[34] and demonstrated in many materials including ruthenates.[20,33,35,36] Materials with itinerant ferromagnetism and cubic-tetragonal-orthorhombic structures are generally characterized by twofold and fourfold anisotropy in AMR, with the minimum magnetoresistivity occurring along the maximal spin polarization direction. For example, the FM state of $SrRuO_3$ film shows twofold anisotropy in its AMR,[35] whereas the azimuthal AMR of FM $Sr_4Ru_3O_{10}$ shows twofold anisotropy below the metamagnetic transition field B_C (~2 T) and fourfold anisotropy above B_C.[33] As indicated above, the fourfold anisotropy of AMR observed in CRO and CSRO#1 films arises from FM anisotropy. The minimum values of AMR should correspond to the least spin-scattering directions. The $\pi/4$ phase shift in AMR (ϕ) from CRO to CSRO#1 suggests that the maximal spin polarization direction under a given field rotates by 45°. Given that spin preferential direction in a magnetic state depends on spin-orbital coupling, the change of easy spin polarization directions from CRO to CRO#1 may be associated with the tuning of spin-orbital coupling by the epitaxial strain. Further studies are needed to fully understand this issue.

Finally, let us discuss why the nearly FM state seen in the $x \sim 0.5$ CSRO bulk material is not further enhanced by epitaxial strain on the CSRO#2 sample. First, previous studies have revealed that the nearly FM state near $x \sim 0.5$ for bulk CSRO is driven by RuO_6 octahedral rotation.[13,17] The octahedral rotation leads the conduction band from the Ru4d_{xy} orbital to become narrow and shift to lower binding energy, which results in the increase of density of state at Fermi level $D(E_F)$ and enhances magnetic fluctuations. In bulk CSRO, the octahedral rotation angle gradually increases with Ca substitution for Sr for $0.5 \leqslant x \leqslant 1.5$ due to smaller ionic radius of Ca^{2+}.[16] Therefore, magnetic fluctuations gradually enhance with the increase of Ca content in this composition region. For $x < 0.5$, the system switches to a state characterized by AFM correlations, which is driven by the RuO_6 octahedral tilting, as noted above. Second, as discussed above, unlike the CRO and CSRO#1 films characterized by compressive strain, the CSRO#2 film shows biaxial tensile strain. From the structural confinement effect imposed by the LAO substrate, we can reasonably expect that the octahedral rotation is suppressed by the tensile strain, which should lead to the decrease of $D(E_F)$ according to the discussions made above. Such a decrease of $D(E_F)$ should weaken Stoner FM instability. Our observation of paramagnetic, Fermi liquid behavior in CSRO#2 is exactly consistent with this interpretation.

IV. CONCLUSION

We have grown epitaxial thin films of CSRO using the PLD method and investigated epitaxial strain effect on electronic and magnetic properties of this system. Our x-ray diffraction analyses reveal that the nature of strain varies with Sr content for CSRO films grown on LAO substrates. The strain is biaxial compressive for the $x = 0$ sample and evolves toward tensile as x increases. In the $x = 0.1$ sample, we observed weakened compressive strain along the a axis and slight tensile strain along the b axis. When x is increased to 0.5, enhanced tensile strain is observed along both a and b directions. In contrast, the strain is relaxed in all of the SRO films on various substrates.

Such a strain evolution can be interpreted from the variation of lattice parameters of bulk materials with Sr content. The epitaxial strain results in a remarkable effect on electronic and magnetic properties of this system. Unlike the Mott-insulating ground state of the bulk materials for $x = 0$ and 0.1 and nearly FM state for $x = 0.5$, the thin-film samples show an itinerant FM state for $x = 0$ and 0.1 and a paramagnetic state with suppressed magnetic fluctuations for $x = 0.5$. All these exotic properties can be understood in light of the control of octahedral rotation and tilting by the strain. Furthermore, the variation of FM anisotropy with Sr content suggests that the spin-orbital coupling may be tuned by the epitaxial strain.

ACKNOWLEDGMENTS

This research is supported by the Department of Defense Army Research Office under Grant No. W911NF0910530.

*Author to whom correspondence should be addressed: zmao@tulane.edu

[1] Y. Maeno, H. Hashimoto, K. Yoshida, S. Nishizaki, T. Fujita, J. G. Bednorz, and F. Lichtenberg, Nature (London) **372**, 532 (1994).
[2] K. Ishida, H. Mukuda, Y. Kitaoka, K. Asayama, Z. Q. Mao, Y. Mori, and Y. Maeno, Nature (London) **396**, 658 (1998).
[3] K. D. Nelson, Z. Q. Mao, Y. Maeno, and Y. Liu, Science **306**, 1151 (2004).
[4] S. Nakatsuji, S. Ikeda, and Y. Maeno, J. Phys. Soc. Jpn. **66**, 1868 (1997).
[5] C. S. Alexander, G. Cao, V. Dobrosavljevic, S. McCall, J. E. Crow, E. Lochner, and R. P. Guertin, Phys. Rev. B **60**, R8422 (1999).
[6] R. G. Moore, V. B. Nascimento, J. Zhang, J. Rundgren, R. Jin, D. Mandrus, and E. W. Plummer, Phys. Rev. Lett. **100**, 066102 (2008).
[7] P. B. Allen, H. Berger, O. Chauvet, L. Forro, T. Jarlborg, A. Junod, B. Revaz, and G. Santi, Phys. Rev. B **53**, 4393 (1996).
[8] S. A. Grigera, R. S. Perry, A. J. Schofield, M. Chiao, S. R. Julian, G. G. Lonzarich, S. I. Ikeda, Y. Maeno, A. J. Millis, and A. P. Mackenzie, Science **294**, 329 (2001).
[9] D. J. Singh and S. Auluck, Phys. Rev. Lett. **96**, 097203 (2006).
[10] W. Bao, Z. Q. Mao, Z. Qu, and J. W. Lynn, Phys. Rev. Lett. **100**, 247203 (2008).
[11] F. Nakamura, T. Goko, M. Ito, T. Fujita, S. Nakatsuji, H. Fukazawa, Y. Maeno, P. Alireza, D. Forsythe, and S. R. Julian, Phys. Rev. B **65**, 220402 (2002).
[12] F. Nakamura, J. Phys. Soc. Jpn. **76**, 96 (2007).
[13] S. Nakatsuji and Y. Maeno, Phys. Rev. Lett. **84**, 2666 (2000).
[14] S. Nakatsuji and Y. Maeno, Phys. Rev. B **62**, 6458 (2000).
[15] S. Ikeda, Y. Maeno, and T. Fujita, Phys. Rev. B **57**, 978 (1998).
[16] O. Friedt, M. Braden, G. André, P. Adelmann, S. Nakatsuji, and Y. Maeno, Phys. Rev. B **63**, 174432 (2001).
[17] Z. Fang and K. Terakura, Phys. Rev. B **64**, 020509 (2001).
[18] R. Ishikawa, H. Taniguchi, S. K. Goh, S. Yonezawa, F. Nakamura, and Y. Maeno, J. Phys.: Conf. Ser. **400**, 022036 (2012).
[19] X. Wang, Y. Xin, P. A. Stampe, R. J. Kennedy, and J. P. Zheng, Appl. Phys. Lett. **85**, 6146 (2004).
[20] L. Miao, P. Silwal, X. Zhou, I. Stern, J. Peng, W. Zhang, L. Spinu, Z. Q. Mao, and D. H. Kim, Appl. Lett. Phys. **100**, 052401 (2012).
[21] P. Steffens, O. Friedt, P. Alireza, W. G. Marshall, W. Schmidt, F. Nakamura, S. Nakatsuji, Y. Maeno, R. Lengsdorf, M. M. Abd-Elmeguid, and M. Braden, Phys. Rev. B **72**, 094104 (2005).
[22] S. Madhavan, D. G. Schlom, A. Dabkowski, H. A. Dabkowska, and Y. Liu, Appl. Phys. Lett. **68**, 559 (1996).
[23] M. A. Zurbuchen, Y. F. Jia, S. Knapp, A. H. Carim, D. G. Schlom, L. N. Zou, and Y. Liu, Appl. Phys. Lett. **78**, 2351 (2001).
[24] D. Reisinger, B. Blass, J. Klein, J. B. Philipp, M. Schonecke, A. Erb, L. Alff, and R. Gross, Appl. Phys. A: Mater Sci. Process. **77**, 619 (2003).
[25] T. Ohnishi and K. Takada, Appl. Phys. Express **4**, 025501 (2011).
[26] Y. Krockenberger, M. Uchida, K. S. Takahashi, M. Nakamura, M. Kawasaki, and Y. Tokura, Appl. Phys. Lett. **97**, 082502 (2010).
[27] W. Tian, J. H. Haeni, D. G. Schlom, E. Hutchinson, B. L. Sheu, M. M. Rosario, P. Schiffer, Y. Liu, M. A. Zurbuchen, and X. Q. Pan, Appl. Phys. Lett. **90**, 022507 (2007).
[28] J. Peng, Z. Qu, B. Qian, D. Fobes, T. J. Liu, X. Wu, H. M. Pham, L. Spinu, and Z. Q. Mao, Phys. Rev. B **82**, 024417 (2010).
[29] M. Braden, G. André, S. Nakatsuji, and Y. Maeno, Phys. Rev. B **58**, 847 (1998).
[30] T. Vogt and D. J. Buttrey, Phys Rev. B **52**, R9843 (1995).
[31] R. Datta, S. Kanuri, S. V. Karthik, D. Mazumdar, J. X. Ma, and A. Gupta, Appl. Phys. Lett. **97**, 071907 (2010).
[32] H. Yamazaki, Y. Hikita, H. Hori, and H. Takagi, Appl. Phys. Lett. **83**, 3740 (2003).
[33] D. Fobes, T. J. Liu, Z. Qu, M. Zhou, J. Hooper, M. Salamon, and Z. Q. Mao, Phys. Rev. B **81**, 172402 (2010).
[34] W. Limmer, M. Glunk, J. Daeubler, T. Hummel, W. Schoch, R. Sauer, C. Bihler, H. Huebl, M. S. Brandt, and S. T. B. Goennenwein, Phys. Rev. B **74**, 205205 (2006).
[35] O. Morán, W. Saldarriaga, and E. Baca, Solid State Sci. **11**, 1187 (2009).
[36] J. Eckstein, I. Bozovic, J. O'Donnell, M. Onellion, and M. Rzchowski, Appl. Phys. Lett. **69**, 1312 (1996).